Molecular Numbers in Core and Shell: Structural Dependence of Reactivity of Alkylcarboxylate-Stabilized Silver Nanoparticles

Nianjun Yang and Koichi Aoki*

Department of Applied Physics, University of Fukui, 3-9-1 Bunkyo, Fukui-shi, 910-8507 Japan

Received: April 26, 2005; In Final Form: August 17, 2005

Spectroscopic, chemical, thermal, and voltammetric analyses on six kinds of alkylcarboxylate-stabilized silver nanoparticles 4.7 nm in diameter were carried out with an aim to reveal the effect of alkylcarboxylates on the optical, thermal, geometric, and electrochemical properties of the nanoparticles. These nanoparticles are composed of silver atoms and silver alkylcarboxylates having even numbers, *m*, of carbon atoms from 8 to 18. As a measure of the structure of the nanoparticles, the ratio of the number of silver atoms (n_{Ag}) to that of alkylcarboxylates (n_s) per nanoparticle was evaluated by means of titration through chemical oxidation, voltammetric currents, and thermal gravimetric analysis. It increased with an increase in *m* and ranged from 1.3 to 9.8. Properties of the nanoparticle have been exhibited in absorbance of the UV−vis spectra at the point of the proportionality to n_{Ag}, voltammetric currents of which values were close to the theoretical values at the diffusion of particle itself, and the *m*-independent kinetic energy of the thermal decomposition and the overpotential of the reduction. They are not observed for the composed species, that is, silver atoms and silver alkylcarboxylate molecules.

Introduction

Nanometer-sized particles of metals, semiconductors, magnetic materials, and polymers are coated necessarily with stabilizers such as thiols/thiolates/sulfides,[1−3] thioether,[4] carboxylates,[5−7] polymers,[8] metals,[9] amino acids,[10] phosphine/phosphonate/phosphate,[6b,11] isocyanide,[12] xanthates,[13] acetone,[14] or iodine[15] to avoid aggregation or precipitation. Selection of stabilizers has influenced the size,[3d,e] shape, and size distribution[1−8] of nanoparticles. Murray et al.[1c] revealed that thiols played a significant role in ripening the gold nanoclusters to form superlattices. Efrima et al.[5] examined the size distribution of silver nanoparticles by altering the chain length, the configuration, and the degree of unsaturation of alkylcarboxylates as stabilizers. Martin et al.[1c] found that the nanoclusters became larger and more polydispersed as the protective alkylthiols were longer. Chen et al.[2e] pointed out that longer alkanethiolates formed more ordered palladium nanoparticles. Zhong et al.[4] succeeded in controlling the size and shape of gold nanoparticles by adopting tridentate thioether as a stabilizer.

Chemical structures of stabilizers have altered the optical,[5a,16] electronic,[17] magnetic,[18] thermal,[19] biological/chemical,[20] and catalytic[21] properties of nanoparticles. Schatz and Van Duyne et al.[16] observed a 3 nm red shift of the localized surface plasmon resonance of silver nanoparticles per carbon atom in alkanethiols. Chaudret et al.[18b] demonstrated that an alkyl aluminum shell provided the low packing density of cobalt nanoparticles as well as a decrease in magnetization, whereas amido aluminum, an electron donor, yielded compact structure and magnetization in bulk. Zhong et al.[20a] applied gold nanoparticles to artificial blocking of chemically sensitive interfaces by use of difference in binding energy of stabilizers.

Removal of stabilizers from nanoparticles causes aggregation to yield thin film and secondary particles. Quinn et al.[22a] reported the electrochemically reductive removal of hexanethiol from gold nanoparticles (Au_{147}) by use of the electrified water/1,2-dichloroethane interface. Zhong et al.[23] removed thermally decanethiolate and 1,9-nonanedithiolate from gold nanoparticles to yield the catalyst for the oxidation of methanol. Some reductive removals were carried out by thermal treatments of metal-carboxylate-bridged gold nanoparticles[24a] for preparing conductive materials, those of surfactant-capped Pt/Ru nanoparticles,[25] those of $PtRu_5C(CO)$[26] immobilized on the carbon plate, those of polymer-mediated assembly of Pd on SiO_2 nanoparticles,[27] those of dendrimer-mediated assembly of metal nanoparticles[28] for preparing catalysts, and those of silver nanoparticles for low-temperature metallization.[29a] Unfortunately, few researchers[29a] have focused on a relationship between the kinetics of the removal of the stabilizer and structure of nanoparticles, to our knowledge.

Silver nanoparticles, stabilized by alkylcarboxylates, are promising for obtaining the above relationship, partly because they are spectroscopically and electrochemically active enough to estimate their structure[29] and partly because monodispersed particles can readily be synthesized by thermal decomposition of silver alkylcarboxylates.[7] Their additional advantage is the flexible variations of the surface energy by altering the chain length of alkylcarboxylates. For example, nanoparticles made of short lengths of silver alkylcarboxylates are predicted to require more surfactants to avoid aggregation than the long ones and to exhibit lower activation energy of thermal decomposition than the long ones. We report here the effect of the chain lengths of alkylcarboxylates on the kinetics of their thermal decomposition and the number of alkylcarboxylates per nanoparticle. The latter is a measure of the structure of silver nanoparticles, obtained by titration through chemical oxidation and cyclic voltammetry as well as thermogravimetric analysis.

Experimental Section

Chemicals and reagents were of analytical grade. Acetonitrile and cyclohexane were treated with molecular sieves 4A 1/8 (Wako, Tokyo, Japan) to remove water. Fatty acids [HOOC-

* Corresponding author (telephone +81-90-8095-1906; fax +/81-776-278494; e-mail d930099@icpc00.icpc.fukui-u.ac.jp).

10.1021/jp052173m CCC: $30.25
Published on Web 11/24/2005

$(CH_2)_{m-2}CH_3$, m = 18, 16, 14, 12, 10, and 8], silver nitrate, tetra-*n*-butylammonium tetrafluoroborate (TBATFB), sodium chloride, and sodium hydroxide were used as received without purification.

The nanoparticles were synthesized by heating silver alkylcarboxylates[7,29] in the following process. The fatty acid dissolved in the 3.0 M hot sodium hydroxide solution was mixed with the silver nitrate solution with equal molar ratio to yield the white precipitate of silver alkylcarboxylate. Heating the dried silver alkylcarboxylate at 250 °C under nitrogen atmosphere for 2 h led to the color change from white to dark purple. The dark purple, crystal-like product was the silver alkylcarboxylate-stabilized nanoparticles.[7,29]

The particle size was characterized with a 200 kV high-resolution transmission electron microscope (HRTEM, JEOL-2000) at magnification of $\sim 3 \times 10^6$. The samples for HRTEM were prepared by spreading a 100 mm^3 drop of cyclohexane including 1 μg of the nanoparticles on a copper grid-supported amorphous carbon film and by evaporating cyclohexane from the thin film.

UV−vis spectroscopy of the cyclohexane-dissolved nanoparticles was performed with a UV-570 spectrometer (JASCO, Tokyo, Japan). All of the spectra were subtracted from the background for the blank solution of cyclohexane.

Electrochemical experiments were performed with a model 1112 potentio/galvanostat (Huso, Kawasaki, Japan) by use of a standard three-electrode system in a one-compartment cell at room temperature. All of the data were collected by in-house software with a computer. The working electrode was a platinum disk electrode, 1.6 mm in diameter. The counter electrode was a Pt wire, and the reference electrode was a $Ag|Ag_xO$ electrode. The potential difference of $Ag|Ag_xO$ from Ag|AgCl in a 3.0 M NaCl solution was −0.055 V. The solvent used for voltammetry was the mixture of cyclohexane and acetonitrile with a volume ratio of 2:98. The solutions including nanoparticles and TBATFB were deaerated with nitrogen gas for at least 20 min.

Thermogravimetric analysis (TGA) was applied to dried powders of the nanoparticle (8−12 mg) with a DTG-60 (Shimazu, Kyoto, Japan). Temperature was scanned from room temperature to 500 °C at the heating rate of 10 °C min^{-1}. Temperature was monitored with a thermocouple located close to the chamber under nitrogen atmosphere.

The density of silver alkylcarboxylates was evaluated from the mass and the excluded volume in a 10 cm^3 water vessel. The weighted aliquot ($\sim$10 mg) of silver alkylcarboxylates was sunk in water, and the increment of the meniscus was read.

Results

General Features. Six kinds of silver alkylcarboxylate-stabilized nanoparticles, abbreviated AgNP-C_m for m = 18, 16, 14, 12, 10, and 8, were mostly spherical with the common diameter of 4.7 ± 0.6 nm, where the error denotes the standard deviation evaluated by counting 250 particles randomly.[29] These nanoparticles were stable against oxidation by air and concentrated nitric acid. They floated on the surface of water but sank in toluene. They showed electrical resistance >10 MΩ, although they include silver metal. These properties are ascribed to the enclosure of the hydrophobic organic layer, which should be alkylcarboxylates on a silver metal core, as illustrated in Figure 1.[29b]

These nanoparticles did not dissolve in the usually available organic solvents such as hexane, toluene, benzene, nitrobenzene, benzonitrile, *o*-bromotoluene, cyclohexane, heptane, dodecane, dichloromethane, chloroform, carbon tetrachloride, methanol, ethanol, 1-butanol, acetone, acetonitrile, formic acid, butyric acid, triethylamine, or *N*,*N*-dimethylformamide. Only cyclohexane dissolved them. The nanoparticles for m = 18, 16, and 14 dissolved immediately, whereas it took several days to dissolve the nanoparticles for m = 12, 10, and 8.

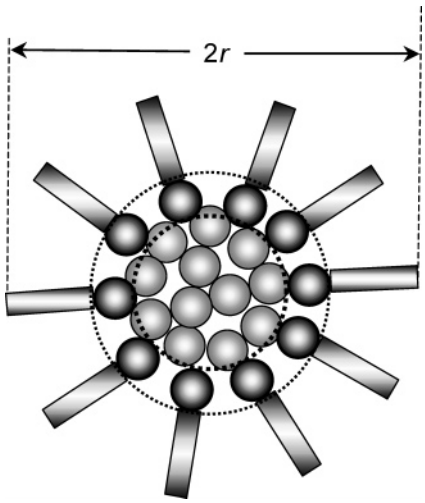

Figure 1. Illustration of structure of silver alkylcarboxylate-stabilized nanoparticle r in radius. The light gray circles and the rectangles are silver atoms in the core, whereas the black circles are the silver alkylcarboxylates in the shell.

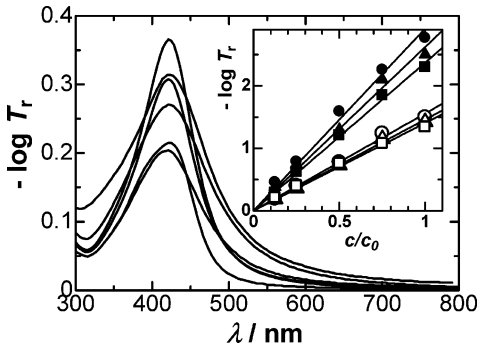

Figure 2. UV spectra of AgNP-C_m, for m = 18, 10, 16, 8, 14, and 12 from top to bottom in cyclohexane solution with the mass concentration of 0.19 mg cm^{-3}. (Inset) Logarithm of the transmittance at 420 nm against the mass concentration of AgNP-C_m, for m = 18 (●), 16 (▲), 14 (■), 12 (○), 10 (△), and 8 (□) for c_0 = 1.50 mg cm^{-3}.

Figure 2 shows the UV spectra of six kinds of nanoparticles dissolved in cyclohexane, where the ordinate is the logarithm of the transmittance, T_r, corresponding to absorbance. The sharp bands appeared at 420 nm. The logarithm of the transmittance was proportional to the weight concentration of each nanoparticle, as is seen in the inset of Figure 2. The band has been attributed to the Mie scattering of nanoparticles for m = 18,[29b] in agreement with the simulated spectrum for nanoparticles 5 nm in diameter.[29b] Because the six kinds of nanoparticles have a common diameter (4.7 nm), their spectra are almost overlapped.

Molecular Ratio in Core to in Shell. We attempted to reduce the nanoparticles with sodium citrate, hydrazine, urotropine, hexamethylenetetramine, dimethyl sulfoxide, or sodium borohydride, but failed. In contrast, the nanoparticles were oxidized with potassium permanganate. When an extra amount of acidic (1.0 M sulfuric acid) potassium permanganate solution (1.0 M) was mixed vigorously with the nanoparticle-included cyclohexane in an emulsion form, a black precipitate appeared and the original purple color disappeared quickly for m = 18, 16, and 14. The oxidation of the nanoparticles for m = 12, 10, and

TABLE 1: Variations of n_{Ag}/n_s, n_{Ag}, and n_s with m

	m:	8	10	12	14	16	18
n_{Ag}/n_s	ChmOx[a]	1.2	1.5	1.9	4.7	6.6	9.8
	ElcC[a]	1.3	1.5	1.8	4.7	6.6	9.6
	TGA	1.3	1.6	1.8	4.7	6.7	9.6
n_{Ag}		480	490	520	1020	1200	1440
n_s		363	325	291	217	180	150
T_m/°C			305	300	302	311	307

[a] ChmOx, chemical oxidation; ElcC, electrochemical analysis.

8 required ultrasonication of the emulsion for at least 5 min. The precipitation for $m = 18$ has been demonstrated to be silver sulfonate from the silver atoms.[29b]

If we assume that the nanoparticle is composed by n_{Ag} silver atoms and n_s silver alkylcarboxylates, the oxidation by permanganate can be expressed by

$$(10/n_{Ag})[n_{Ag}Ag - n_s(AgC_m)] + 2MnO_4^- + 16H^+ + 5SO_4^{2-} \rightarrow 5Ag_2SO_4 + 2Mn^{2+} + 8H_2O + 10(n_s/n_{Ag})(AgC_m) \quad (1)$$

The amount of silver sulfonate was substituted with silver chloride by titrating sodium chloride solution until the black precipitate disappeared through the reaction

$$Ag_2SO_4 + 2Cl^- \rightarrow 2AgCl\downarrow + SO_4^{2-} \quad (2)$$

The precipitation of silver chloride was filtered, rinsed with methanol and with water, dried, and weighed. Letting k be the number of nanoparticles before the oxidation, the molar number of silver chloride is given by kn_{Ag}/N_A, in which N_A is the Avogadro constant. This value corresponds to the dried weight of silver chloride, W_{AgCl}, expressed as

$$W_{AgCl} = M_{AgCl}kn_{Ag}/N_A \quad (3)$$

where M_{AgCl} is the molecular weight of silver chloride. This yields a value of kn_{Ag} from W_{AgCl}. Letting the weight of the nanoparticles before the oxidation be W_{NP}, we can express the weight of one nanoparticle as

$$W_{NP} = k(n_{Ag}M_{Ag} + n_sM_s)/N_A \quad (4)$$

where $(n_{Ag}M_{Ag} + M_sn_s)$ is the average weight of the N_A nanoparticles. M_s and M_{Ag} are the molecular weights of silver alkylcarboxylates [$(139 + 14m)$ g mol^{-1}] and silver (108 g mol^{-1}), respectively. Multiplying N_A/kM_sn_{Ag} onto both sides of eq 4 and extracting n_s/n_{Ag}, we have

$$n_s/n_{Ag} = W_{NP}N_A/kn_{Ag}M_s - M_{Ag}/M_s \quad (5)$$

Eliminating kn_{Ag} in eq 5 by use of eq 3 yields

$$n_s/n_{Ag} = W_{NP}M_{AgCl}/W_{AgCl}M_s - M_{Ag}/M_s \quad (6)$$

Values of all of the variables on the right-hand side are known. As a measure of the composition of nanoparticles, we evaluated n_{Ag}/n_s for six kinds of nanoparticles and listed them in Table 1. They increase with an increase in m.

Thermal Reactivity. When six kinds of nanoparticles were heated at 250 °C in air for 10 min, the crystal-like and purple powders changed to brilliant white grains or powders with the density of 9.0 g cm^{-3}, evaluated from the previous method for silver stearate-stabilized nanoparticles.[29a] Further heating at higher temperature yielded the fused metal-like solid having the same density as silver bulk (10.5 g cm^{-3}). The film of brilliant white powders on the indium−tin oxide surface in cyclohexane showed the absorbance band at 420 nm, whereas that of the fused solid did not.[29a] This temperature turning between two states is defined as the metallization temperature, T_m. Table 1 lists the variation of T_m with m, showing the independence of m. Because the appearance, densities, and T_m are common to the six nanoparticles, the particles over 250 °C may have identical structure.

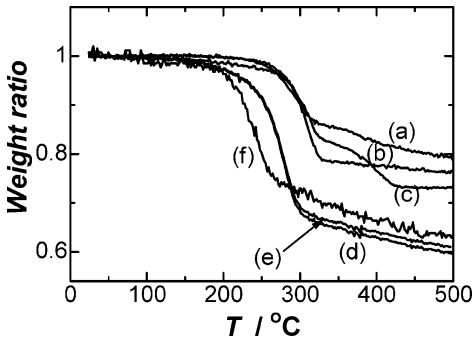

Figure 3. Thermograms for AgNP-C$_m$, for m = (a) 18, (b) 16, (c) 14, (d) 12, (e) 10, and (f) 8 at the heating rate of 10 °C min^{-1} under nitrogen atmosphere.

To investigate the kinetics of the metallization of the nanoparticles, we performed TGA for six nanoparticles under nitrogen atmosphere. The thermograms in Figure 3 show that the nanoparticles lost weight in the temperature range from 200 to 340 °C. The weight ratios of the remnant were 80, 76, 73, 60, 62, and 64% for $m = 18$, 16, 14, 12, 10, and 8, respectively. The remnants, being cooled under nitrogen atmosphere, were white powders. The weight loss for $m = 18$ has been attributed to the decomposition of the nanoparticles into silver metals and gas[29a] according to

$$AgNP\text{-}C_m \rightarrow Ag + gas \quad (7)$$

The weights of the nanoparticles before and after the thermal decomposition are, respectively, given by $k(n_sM_s + n_{Ag}M_{Ag})/N_A$ and $k(n_s + n_{Ag})M_{Ag}/N_A$. Taking the ratio of two weights, we obtain

$$s = (n_s + n_{Ag})M_{Ag}/(n_sM_s + n_{Ag}M_{Ag}) \quad (8)$$

and rewrite it to

$$n_{Ag}/n_s = (sM_s - M_{Ag})/(1 - s)M_{Ag} \quad (8')$$

The values of n_{Ag}/n_s were evaluated from the weight ratios and are listed in Table 1.

If the nanoparticles are closely packed with silver alkylcarboxylates and silver atoms and if densities of silver atoms, d_{Ag}, and silver alkylcarboxylates, d_s, in the nanoparticles are the same as those in the bulk, respectively, the total volume can be expressed by the summation of the volumes of silver atoms and silver alkylcarboxylates

$$4\pi r^3/3 = (M_{Ag}/d_{Ag})(n_{Ag}/N_A) + (M_s/d_s)(n_s/N_A) \quad (9)$$

where r is the radii of the nanoparticle. Values of d_s were obtained as described under the Experimental Section. Eliminating n_s in eq 9 by use of β ($= n_{Ag}/n_s$), we obtain

$$n_{Ag} = (4\pi r^3/3)\, N_A/[M_{Ag}/d_{Ag} + (M_s/\beta d_s)] \quad (10)$$

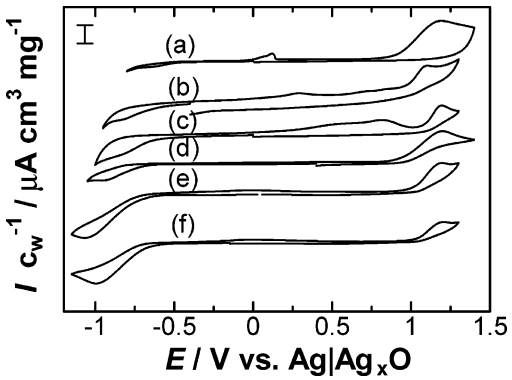

Figure 4. Cyclic voltammograms of AgNP-C$_m$, for m = (a) 18, (b) 16, (c) 14, (d) 12, (e) 10, and (f) 8 at the platinum disk electrode in the 0.1 M TBATFB mixed solvent of acetonitrile and cyclohexane at the scan rate of 10 mV s^{-1}. The current scale was normalized by the mass concentration of the nanoparticles. The measure bar indicates 1 μA mg^{-1} cm^3.

Eliminating n_{Ag} in eq 9 yields

$$n_s = (4\pi r^3/3)\, N_A/[M_s/d_s + \beta(M_{Ag}/d_{Ag})] \qquad (10')$$

The calculated values of n_{Ag} and n_s for six nanoparticles are listed in Table 1. The values of n_s decrease with an increase in m, whereas those of n_{Ag} decrease with a decrease in m.

Electrochemical Reactivity. Figure 4 shows the cyclic voltammograms for six kinds of nanoparticles dissolved in the mixed solvent. The voltammograms include a large anodic wave at ~1.2 V, a small anodic wave in the range from 0.1 to 0.5 V, and a cathodic wave in the domain from −0.6 to −1.05 V. These waves at the second and succeeding potential scans were very similar to those at the first scan. The anodic wave had no effect on the scan in the negative potential domain and vice versa. The peak currents of the anodic wave at ~1.2 V and the cathodic wave were proportional to the concentration of the nanoparticles without significant peak potential shift or shape deformation. Therefore, these anodic and cathodic waves were assigned, respectively, to the oxidation of the silver atoms and the reduction of Ag^+ in the moiety of silver alkylcarboxylates.[29a,c] The anodic peak potentials were independent of m, whereas the cathodic ones shifted positively with a decrease in m. This shift has been attributed to the variation of silver alkylcarboxylates with the interaction between silver atoms in −Ag−AgOOC-$(CH_2)_{m-2}CH_3$.[29c] Because silver metal started to be dissolved at 0.05 V in the mixed solvent,[29c] the potential difference between the reactions $Ag^+ + e^- \rightarrow Ag$ and $AgC_m + e^- \rightarrow Ag + C_m^-$ ranges from 0.65 to 1.10 V, depending on m. The shift can be ascribed to the high stability of silver carboxylates. It leads to the estimation of the stability constant from 10^{13} to 10^{21}.

Figure 5 shows plots of the peak currents of the anodic wave at ~1.2 V and the cathodic wave against the square root of the potential scan rates, v. Good proportionality was found. This proportionality as well as the proportionality to the concentration indicates that the peak currents should be controlled by diffusion of the nanoparticles. The peak currents, I_p, for the diffusion-controlled nanoparticles having n redox sites has been expressed by[30]

$$I_p = 0.446nFcA(DvF/RT)^{1/2} \qquad (11)$$

where D is the diffusion coefficient of the nanoparticle and the other variables have conventional meanings. Values of c, D, and v should be common to those for the anodic and cathodic

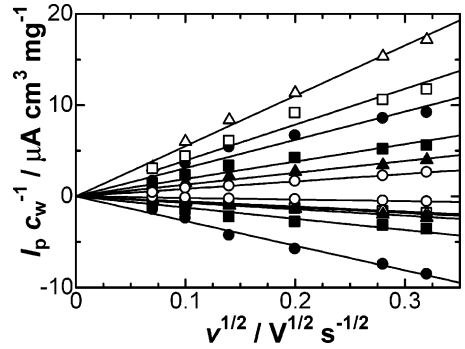

Figure 5. $v^{1/2}$ dependence of the concentration-normalized peak currents, $I_p c_w^{-1}$, of the anodic wave at ~1.2 V and the cathodic wave at the potential range from −0.6 to −1.05 V for AgNP-C$_m$ with m = 18 (△), 16 (□), 14 (○), 12 (▲), 10 (■), and 8 (●) in the 0.1 M TBATFB mixed solvent of acetonitrile and cyclohexane.

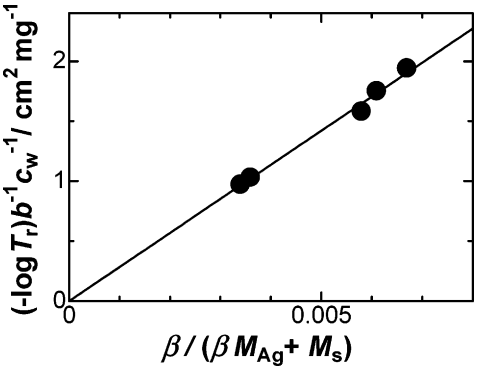

Figure 6. Variation of $(-\log T_r)/bc_w$ with $\beta/(\beta M_{Ag} + M_s)$.

peak currents. Only the difference in both currents lies in n. Because the anodic peak currents result from the oxidation of silver, the value of n for the oxidation stands for the number of silver atoms, n_{Ag}, per nanoparticle. On the other hand, the value of n for the reduction represents the number of silver alkylcarboxylates, n_s, per nanoparticle. The ratio of the anodic peak current to the cathodic one in eq 10 is equal to n_{Ag}/n_s. These values determined from the slope in Figure 5 are shown in Table 1. They agree with the values obtained from TGA and the titration by chemical oxidation.

Discussion

Spectroscopy. The wavelength of the bands was independent of m, whereas the transmittance varied with the concentration as well as m (in the inset of Figure 2). Because the intensity of the Mie scattering is proportional to the amount of scattering species, we can represent the intensity in the same form as in the light absorption, that is, the Lambert−Beer law. We define the transmittance coefficient per nanoparticle, ϵ, in the same manner as the molar absorption coefficient to be

$$-\log T_r = \epsilon b N_A c_w/(n_{Ag}M_{Ag} + n_s M_s) \qquad (12)$$

where b is the optical length (1 cm) and c_w is the weight concentration of nanoparticles. When the weight concentration is represented by the molar concentration [$c_w = c(n_{Ag}M_{Ag} + n_s M_s)$], eq 12 is written as

$$(-\log T_r)/bc_w = \epsilon n_{Ag} N_A \beta/(\beta M_{Ag} + M_s) \qquad (12')$$

The left-hand side is equivalent to the slopes in the inset of Figure 2. It is plotted against $\beta/(\beta M_{Ag} + M_s)$ in Figure 6. The proportionality indicates that ϵn_{Ag} be a characteristic variable

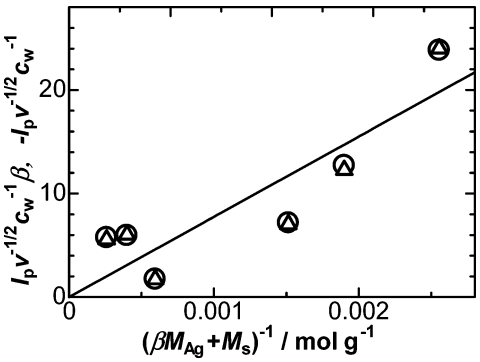

Figure 7. Plots of $I_p/c_w v^{1/2}\beta$ (△) and $-I_p/c_w v^{1/2}$ (○) against $(\beta M_{Ag} + M_s)^{-1}$.

common to the six nanoparticles. The inclusion of n_{Ag} in the invariant parameter ϵn_{Ag} means that the scattering is caused by silver atoms in the core rather than the whole sphere of the nanoparticle.

Electrochemistry. We tried to estimate the absolute values of the peak currents. Equation 10 in which c is replaced by $c_w/(n_{Ag}M_{Ag} + n_sM_s)$ can be rewritten as

$$I_p/(c_w v^{1/2}) = 0.446nFA(DF/RT)^{1/2}/(n_{Ag}M_{Ag} + n_sM_s) \quad (13)$$

Replacing n for the anodic and cathodic peak currents by n_{Ag} and n_s, respectively, in eq 13, we obtain

$$(I_p)_A/c_w v^{1/2}\beta = 0.446FA(DF/RT)^{1/2}/(\beta M_{Ag} + M_s) \quad (14)$$

$$(I_p)_C/c_w v^{1/2} = -0.446FA(DF/RT)^{1/2}/(\beta M_{Ag} + M_s) \quad (14')$$

By use of the known slopes in Figure 5 and β, values on the left-hand side of eqs 14 and 14′ were plotted against $(\beta M_{Ag} + M_s)^{-1}$ in Figure 7. Although the data were rather scattered, a proportional line was drawn compulsively. The slope was 7.8 A cm^3 mol^{-1} s$^{1/2}$ V$^{-1/2}$. This value is close to the theoretical value, 8.4 A cm^3 mol^{-1} s$^{1/2}$ V$^{-1/2}$ for $0.446FA(DF/RT)^{1/2}$ in eq 14 when D was evaluated to be 0.25×10^{-5} cm^2 s^{-1} from the Stokes−Einstein equation for the particle radius 2.35 nm and the viscosity of acetonitrile (0.39 mPa s). The similarity between the experimental and theoretical values indicates that the nanoparticles should behave electrochemically as multiple charged redox species; that is, they are being transported to the electrode by physical diffusion, colliding with the electrode surface, and transferring all of the charge rather than the partial charge transfer of ferrocene-immobilized polystyrene particles.[32]

Thermal Gravimetric Analysis. We evaluate here the activation energy for the decomposition of the nanoparticles by analyzing the thermograms of the weight loss versus temperature. The thermal decomposition of the nanoparticle into silver and gas, given by eq 7, has been assumed to be first-order,[29a] the reaction rate constant having the Arrhenius type activation energy, U. When the nanoparticles are heated at a given rate, u, of increasing temperature, the time-dependent kinetics equation can be expressed approximately in terms of the weight loss as a function of temperature, T[29a]

$$\ln\{\ln[(w_0 - w_f)/(w_t - w_f)]/T^2\} = \ln(A_0R/uT) - U/RT \quad (15)$$

where A_0 is the frequency factor and w_0, w_t, and w_f are the initial mass, the mass at T, and the final mass of the samples, respectively. Plots of $\ln\{\ln[(w_0 - w_f)/(w_t - w_f)]/T^2\}$ versus T^{-1}

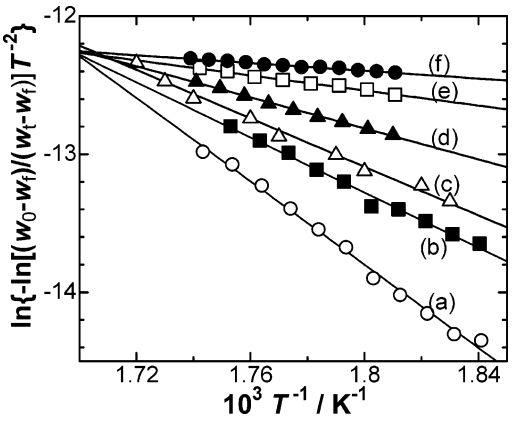

Figure 8. Plots of the term on the left side in eq 15 against T^{-1} for m = (a) 18, (b) 16, (c) 14, (d) 12, (e) 10, and (f) 8.

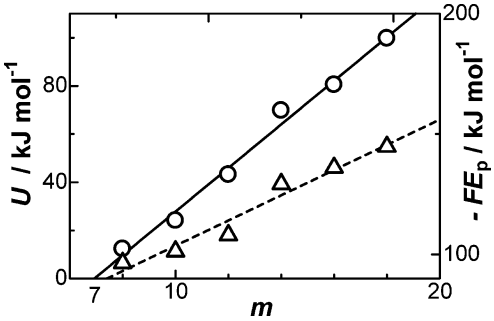

Figure 9. m dependence of (○) the activation energy, U, for the thermal decomposition, and (△) the dissociation energy of silver alkylcarboxylate molecules obtained by voltammetric peak potentials.[29c]

in Figure 8 fall on straight lines in the domain from 270 to 320 °C. We obtained values of the activation energy from the slope of the lines.

Figure 9 presents the variation of the activation energy with m, showing a linear relationship with m. When $m = 7$, the activation energy might be 0. Therefore, no nanoparticle can be synthesized by the thermal decomposition for $m \leq 7$. The increase in the activation energy with m is consistent with the increasing variations of the crystallization energy and the dissociation potential of fatty acids (triangles in Figure 9).[29c] This similarity corresponds to the free energy relationship between kinetic energy and equilibrium free energy. The slope, 9 kJ mol^{-1}, means the increment of activation energy per methylene chain of alkylcarboxylates, which is slightly larger than the dissociation energy of silver alkylcarboxylate molecules (5.2 kJ mol^{-1}) per methylene.

It is interesting to discuss the activation energy per particle rather than per alkylcarboxylate molecule. If the activation energy per particle is allowed to be expressed as the simple summation of each energy, it is given by n_sU and is plotted against m in Figure 10. The total activation energies (circles) increase with an increase in m for $m = 8-12$ and reach the highest for $m = 14-18$. The independence of m for $14 \leq m \leq 18$ implies that the nanoparticles should be stabilized against thermal decomposition by taking the adequate values of n_{Ag} and n_s in the course of the synthesis.

It is predicted that other kinetic energies per particle also reach maximum for $m = 14-18$. As the kinetic energy available, we can use the difference of the voltammetric peak potential of nanoparticles from that of silver alkylcarboxylate molecules.[29c] Figure 10 (triangles) shows m dependence of the potential difference, ΔE_p, on the same scale as the n_sU by multiplying

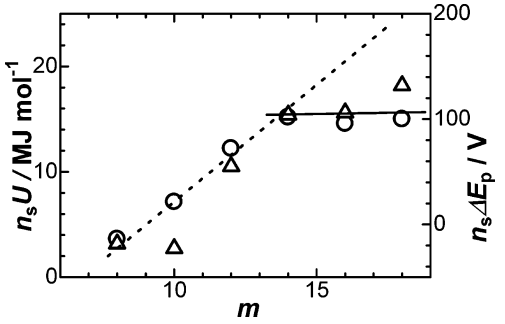

Figure 10. m dependence of n_sU ($\pm$) and the difference of the voltammetric peak potential of nanoparticles (triangle) from that of silver alkylcarboxylate molecules, ΔE_p. The scale on the right ordinate is equivalent to the scale on the left by multiplying F.

by F. The dependence is similar to that of n_sU, indicating that the nanoparticles are also stabilized against electrode kinetics for $m \geq 14$.

Conclusion

Silver nanoparticles were composed of silver metal and silver alkylcarboxylate. The ratios, n_{Ag}/n_s ($= \beta$), were evaluated from the titration by chemical oxidation, voltammetric currents, and the weight change by the thermal decomposition. These techniques are essentially common in that they are caused by redox reactions, that is, the titration being due to oxidation of the silver core, the voltammetry being due to the oxidation of the silver core and the reduction of the silver carboxylate shell, and the TGA being due to thermal reduction of the silver carboxylate shell. The agreement among the three methods justifies these values. These values increase with an increase in m, implying lower density of alkylcarboxylates. Because the stability constants of alkylcarboxylates increase with m, even a few alkylcarboxylate molecules can stabilize nanoparticles.

Properties of the nanoparticle itself have been exhibited in absorbance of the UV−vis spectra at the point of the proportionality to n_{Ag}, voltammetric currents of which values were close to the theoretical values at the diffusion of particle itself, and the m-independent kinetic energy of the thermal decomposition and the overpotential of the reduction. They are not observed from the composed species, that is, silver atoms and silver alkylcarboxylate molecules.

References and Notes

(1) (a) Chen, S.; Murray, R. W. *Langmuir* **1999**, *15*, 682−689. (b) Templeton, A. C.; Chen, S.; Gross, S. M.; Murray, R. W. *Langmuir* **1999**, *15*, 66−76. (c) Martin, J. E.; Wilcoxon, J. P.; Odinek, J.; Provencio, P. *J. Phys. Chem. B* **2000**, *104*, 9475−9486.

(2) (a) Chen, S.; Pei, R.; Zhao, T.; Dyer, D. J. *J. Phys. Chem. B* **2002**, *106*, 1903−1908. (b) Chen, S.; Sommers, J. M. *J. Phys. Chem. B* **2001**, *105*, 8816−8820. (c) Yang, Y.; Grant, K. M.; White, H. S.; Chen, S. *Langmuir* **2003**, *19*, 9446−9449. (d) Chen, S.; Huang, K. *Langmuir* **2000**, *16*, 2014−2018. (e) Chen, S.; Huang, K.; Stearns, J. A. *Chem. Mater.* **2000**, *12*, 540−547.

(3) (a) Han, L.; Luo, J.; Kariuki, N. N.; Maye, M. M.; Jones, V. W.; Zhong, C. J. *Chem. Mater.* **2003**, *15*, 29−37. (b) Kariuki, N. N.; Han, L.; Ly, N. K.; Patterson, M. J.; Maye, M. M.; Liu, G.; Zhong, C. J. *Langmuir* **2002**, *18*, 8255−8259. (d) Shelley, E. J.; Ryan, D.; Johnson, S. R.; Couillard, M.; Fitzmaurice, D.; Nellist, P. D.; Chen, Y.; Palmer, R. E.; Preece, J. A. *Langmuir* **2002**, *18*, 1791−1795. (e) Manna, A.; Imae, T.; Iida, M.; Hisamatsu, N. *Langmuir* **2001**, *17*, 6000−6004.

(4) (a) Maye, M. M.; Chun, S. C.; Han, L.; Rabinovich, D.; Zhong, C. J. *J. Am. Chem. Soc.* **2002**, *124*, 4958−4959. (b) Maye, M. M.; Lim, I.-I. S.; Luo, J.; Rab, Z.; Rabinovich, D.; Liu, T.; Zhong, C. J. *J. Am. Chem. Soc.* **2005**, *127*, 1519−1529. (c) Maye, M. M.; Luo, J.; Lim, I.-I. S.; Han, L.; Kariuki, N. N.; Rabinovich, D.; Liu, T. B.; Zhong, C. J. *J. Am. Chem. Soc.* **2003**, *125*, 9906−9907. (d) Jin, Y.; Dong, S. *J. Phys. Chem. B* **2003**, *107*, 12902−12905.

(5) (a) Wang, W.; Chen, X.; Efrima, S. *J. Phys. Chem. B* **1999**, *103*, 7238−7246. (b) Bradley, M.; Krech, J.; Efrima, S. *J. Phys. Chem.* **1995**, *99*, 292−300. (c) Pradhan, N.; Katz, B.; Efrima, S. *J. Phys. Chem. B* **2003**, *107*, 13843−13854. (d) Wang, W.; Efrima, S.; Regev, O. *Langmuir* **1998**, *14*, 602−610.

(6) (a) Wu, N.; Fu, L.; Su, M.; Aslam, M.; Wong, K. C.; Dravid, V. P. *Nano Lett.* **2004**, *4*, 383−386. (b) Sahoo, Y.; Pizem, H.; Fried, T.; Golodnitsky, D.; Burstein, L.; Sukenik, C. N.; Markovich, G. *Langmuir* **2001**, *17*, 7907−7911. (c) Lin, S.-Y.; Tsai, Y.-T.; Chen, C.-C.; Lin, C.-M.; Chen, C.-H. *J. Phys. Chem. B* **2004**, *108*, 2134−2139. (d) Kataby, G.; Cojocaru, M.; Prozorov, R.; Gedanken, A. *Langmuir* **1999**, *15*, 1703−1708. (e) Chen, S.; Kimura, K. *Langmuir* **1999**, *15*, 1075−1082.

(7) (a) Nagasawa, H.; Maruyama, M.; Komatsu, T.; Isoda, S.; Kobayashi, T. *Phys. Stat. Sol.* **2002**, *191*, 67−71. (b) Kuwajima, S.; Okada, Y.; Yoshida, Y.; Abe, K.; Tanigaki, N.; Yamaguchi, T.; Nagasawa, H.; Sakurai, K.; Yase, K. *Colloids Surf. A* **2002**, *197*, 1−5. (c) Nagasawa, H.; Nakamoto, M.; Yase, K.; Yamaguchi, T. *Mol. Cryst. Liq. Cryst.* **1998**, *322*, 179−184. (d) Abe, K.; Hanada, T.; Yoshida, Y.; Tanigaki, N.; Takiguchi, H.; Nagasawa, H.; Nakamoto, M.; Yamaguchi, T.; Yase, K. *Thin Soid Films* **1998**, *327*, 524−527.

(8) (a) Shim, S. E.; Lee, H.; Choe, S. *Macromolecules* **2004**, *37*, 5565−5571. (b) Yang, L.; Luo, Y.; Jia, X.; Ji, Y.; You, L.; Zhou, Q.; Wei, Y. *J. Phys. Chem. B* **2004**, *108*, 1176−1178. (c) Shan, J.; Chen, J.; Nuopponen, M.; Tenhu, H. *Langmuir* **2004**, *20*, 4671−4676. (d) Wu, X. C.; Bittner, A. M.; Kern, K. *J. Phys. Chem. B* **2005**, *109*, 230−239. (e) Schuetz, P.; Caruso, F. *Chem. Mater.* **2004**, *16*, 3066−3073. (f) Sun, X.; Dong, S.; Wang, E. *Macromolecules* **2004**, *37*, 7105−7108.

(9) (a) Wu, M.-L.; Chen, D.-H.; Huang, T.-C. *Langmuir* **2001**, *17*, 3877−3883. (b) Kariuki, N. N.; Luo, J.; Maye, M. M.; Hassan, S. A.; Menard, T.; Naslund, H. R.; Lin, Y.; Wang, C.; Engelhard, M. H.; Zhong, C.-J. *Langmuir* **2004**, *20*, 11240−11246. (c) Harpeness, R.; Gedanken, A. *Langmuir* **2004**, *20*, 3431−3434. (d) Fleming, M. S.; Walt, D. R. *Langmuir* **2001**, *17*, 4836−4843.

(10) (a) Zhong, Z.; Patskovskyy, S.; Bouvrette, P.; Luong, J. H. T.; Gedanken, A. *J. Phys. Chem. B* **2004**, *108*, 4046−4052. (b) Selvakannan, P. R.; Mandal, S.; Phadtare, S.; Pasricha, R.; Sastry, M. *Langmuir* **2003**, *19*, 3545−3549.

(11) (a) Weare, W. W.; Reed, S. M.; Warner, M. G.; Hutchison, J. E. *J. Am. Chem. Soc.* **2000**, *122*, 12890−12891. (b) Yamamoto, M.; Nakamoto, M. *Chem. Lett.* **2003**, *32*, 452−453.

(12) (a) Chen, J.; Calvet, L. C.; Reed, M. A.; Carr, D. W.; Grushiba, D. S.; Bennett, D. W. *Chem. Phys. Lett.* **1999**, *313*, 741. (b) Kim, H. S.; Lee, S. J.; Kim, N. H.; Yoon, J. K.; Park, H. K.; Kim, K. *Langmuir* **2003**, *19*, 6701−6710. (c) Joo, S.-W.; Kim, W.-J.; Yoon, W. S.; Choi, I. S. *J. Raman Spectrosc.* **2003**, *34*, 271−275.

(13) (a) Tzhayik, O.; Sawant, P.; Efrima, S.; Kovalev, E.; Klug, J. T. *Langmuir* **2002**, *18*, 3364−3369. (b) Pradhan, N.; Katz, B.; Efrima, S. *J. Phys. Chem. B* **2003**, *107*, 13843−13854.

(14) Li, G.; Lauer, M.; Schulz, A.; Boettcher, C.; Li, F.; Fuhrhop, J.-H. *Langmuir* **2003**, *19*, 6483−6491.

(15) Cheng, W.; Dong, S.; Wang, E. *Angew. Chem., Int. Ed.* **2003**, *42*, 449−452.

(16) (a) Malinsky, M. D.; Kelly, K. L.; Schatz, G. C.; Van Duyne, R. P. *J. Am. Chem. Soc.* **2001**, *123*, 1471−1482. (b) Haes, A. J.; Zou, S.; Schatz, G. C.; Van Duyne, R. P. *J. Phys. Chem. B* **2004**, *108*, 6961−6968. Ghosh, S. K.; Nath, S.; Kundu, S.; Esumi, K.; Pal, T. *J. Phys. Chem. B* **2004**, *108*, 13963−13971. (c) Zhang, H.; Zhou, Z.; Yang, B.; Gao, M. *J. Phys. Chem. B.* **2003**, *107*, 8−13.

(17) (a) Brennan, J. L.; Branham, M. R.; Hicks, J. F.; Osisek, A. J.; Donkers, R. L.; Georganopoulou, D. G.; Murray, R. W. *Anal. Chem.* **2004**, *76*, 5611−5619. (b) Ahn, H.; Chandekar, A.; Kang, B.; Sung, C.; Whitten, J. E. *Chem. Mater.* **2004**, *16*, 3274−3278. (c) Chaki, N. K.; Aslam, M.; Gopakumar, T. G.; Sharma, J.; Pasricha, R.; Mulla, I. S.; Vijayamohanan, K. *J. Phys. Chem. B* **2003**, *107*, 13567−13574.

(18) (a) Ely, T. O.; Amiens, C.; Chaudret, B.; Snoeck, E.; Verelst, M.; Respaud, M.; Broto, J.-M. *Chem. Mater.* **1999**, *11*, 526−529. (b) Margeat, O.; Amiens, C.; Chaudret, B.; Lecante, P.; Benfield, R. E. *Chem. Mater.* **2005**, *17*, 107−111.

(19) Badia, A.; Cuccia, L.; Demers, L.; Morin, F.; Lennox, R. B. *J. Am. Chem. Soc.* **1997**, *119*, 2682−2692.

(20) (a) Han, L.; Daniel, D. R.; Maye, M. M.; Zhong, C. J. *Anal. Chem.* **2001**, *73*, 4441−4449. (b) Motte, L.; Pileni, M. P. *J. Phys. Chem. B* **1998**, *102*, 4104−4109. (c) Osman, M. A.; Ernst, M.; Meier, B. H.; Suter, U. W. *J. Phys. Chem. B* **2002**, *106*, 653−662. (d) Bensebaa, F.; Ellis, T. H.; Kruus, E.; Voicu, R.; Zhou, Y. *Langmuir* **1998**, *14*, 6579−6587.

(21) (a) Obrey, S. J.; Barron, A. R. *Macromolecules* **2002**, *35*, 1499−1503. (b) Maye, M. M.; Luo, J.; Lin, Y.; Engelhard, M. H.; Hepel, M.; Zhong, C. J. *Langmuir* **2003**, *19*, 125−131. (c) Luo, J.; Jones, V. W.; Maye, M. M.; Han, L.; Kariuki, N. N.; Zhong, C. J. *J. Am. Chem. Soc.* **2002**, *124*, 13988−13989. (d) Ang, T. P.; Wee, T. S. A.; Chin, W. S. *J. Phys. Chem. B* **2004**, *108*, 11001−11010. (e) Pan, C.; Pelzer, K.; Philippot, K.; Chaudret, B.; Dassenoy, F.; Lecante, P.; Casanove, M.-J. *J. Am. Chem. Soc.* **2001**, *123*, 7584−7593.

(22) (a) Quinn, B. M.; Kontturi, K. *J. Am. Chem. Soc.* **2004**, *126*, 7168−7169. (b) Rapoport, L.; Bilik, Yu.; Feldman, Y.; Homyonfer, M.; Cohen, S. R.; Tenne, R. *Nature* **1997**, *387*, 791−793.

(23) (a) Luo, J.; Jones, V. W.; Maye, M. M.; Han, L.; Kariuki, N. N.; Zhong, C. J. *J. Am. Chem. Soc.* **2002**, *124*, 13988−13989. (b) Luo, J.; Maye, M. M.; Han, L.; Kariuki, N. N.; Jones, V. W.; Lin, Y.; Engelhard, M. H.; Zhong, C. J. *Langmuir* **2004**, *20*, 4254−4260. (c) Luo, J.; Jones, V. W.; Han, L.; Maye, M. M.; Kariuki, N. N.; Zhong, C. J. *J. Phys. Chem. B* **2004**, *108*, 9669−9677.

(24) (a) Wuelfing, W. P.; Zamborini, F. P.; Templeton, A. C.; Wen, X. G.; Yoon, H.; Murray, R. W. *Chem. Mater.* **2001**, *13*, 87−95. (b) Li, Y.; Wu, Y.; Ong, B. S. *J. Am. Chem. Soc.* **2005**, *127*, 3266−3267.

(25) Paulus, U. A.; Endruschat, U.; Feldmeyer, G. J.; Schmidt, T. J.; Bonnemann, H.; Behm, R. J. *J. Catal.* **2000**, *195*, 383−393.

(26) Nashner, M. S.; Frenkel, A. I.; Somerville, D.; Hills, C. W.; Shapley, J. R.; Nuzzo, R. G. *J. Am. Chem.* Soc. **1998**, *120*, 8093−8101.

(27) (a) Galow, T. H.; Drechsler, U.; Hanson, J. A.; Rotello, V. M. *Chem. Commun.* **2002**, 1076−1077. (b) Shenhar, R.; Rotello, V. M. *Acc. Chem. Res.* **2003**, *36*, 549−561. (c) Sun, L.; Crooks, R. M. *Langmuir* **2002**, *18*, 8231−8236.

(28) Yoo, J. W.; Hathcock, D.; El-Sayed, M. A. *J. Phys. Chem. A* **2002**, *106*, 2049−2054.

(29) (a) Yang, N.; Aoki, K.; Nagasawa, H. *J. Phys. Chem. B* **2004**, *108*, 15027−15032. (b) Aoki, K.; Chen, J.; Yang, N.; Nagasawa, H. *Langmuir* **2003**, *19*, 9904−9909. (c) Yang, N.; Aoki, K. *Electrochim. Acta* **2005**, *50*, 4868−4872.

(30) (a) Aoki, K.; Chen, J.; Ke, Q.; Armes, S. P.; Randall, D. P. *Langmuir* **2003**, *19*, 5511−5516. (b) Gao, Y.; Chen, J. *J. Electroanal. Chem.* **2005**, *578*, 129−136. Aoki, K. *Electroanalysis* **2005**, *17*, 1379−1383.

(31) (a) Lee, S. J.; Han, S. W.; Choi, H. J.; Kim, K. *J. Phys. Chem. B* **2002**, *106*, 2892−2900. (b) Lin, B.; Dong, J.; Whitcomb, D. R.; McCormick, A. V.; Davis, H. T. *Langmuir* **2004**, *20*, 9069−9074.

(32) (a) Xu, C.; Chen, J.; Aoki, K. *Electrochem. Comm.* **2003**, *5*, 506−510. (b) Xu, C.; Aoki, K. *Langmuir* **2004**, *20*, 10194−10199. (c) Chen, J.; Zhang, Z. *J. Electroanal. Chem.* **2005**, *583*, 116−123.